Simulating the Perturbation Effects Within an Under-expanded Supersonic Jet

Frederick Ferguson, Yang Gao and Dehua Feng
North Carolina Agricultural and Technical State University,
Greensboro, North Carolina, 27411, U.S.A
fferguso@ncat.edu

Abstract

The transient development of the under-expanded flow field produced by a supersonic jet have drawn considerable interest in the aerodynamic design community. Most recently, this highly unsteady compressible flow has been the subject of numerous computational fluid dynamic (CFD) investigations. Many of which involved the use of unsteady Reynolds Average Navier-Stokes (URANS) equations, Large Eddy Simulation (LES) techniques, Direct Numerical Simulations (DNS) techniques and even the recently developed Gas-Kinetic Scheme (GKS). In general, the most accurate of these CFD simulations obtained from either planar or three-dimensional fields showed the under-expanded flow field features consist of the following: the main vortex pair, vortex-induced shock waves, shock-vortex interactions, and Kelvin-Helmholtz type structures and their evolutions. However, many uncertainties remain at this point. The most important of which is the CFD requirements needed to effectively simulate this highly transient flow field. Moreover, when the technical goal is to gain an understanding of jet-inlet perturbations and their relationship to the vortex-induced shocks within the jet shear layer, as well as, their ability to accelerate the instabilities within the shear layer, the physics capturing capability of CFD techniques becomes even more critical. The objective of this paper is to demonstrate that the 2D Integro-Differential Scheme (IDS) captures the unsteady flow features generated by an under-expanded jet within expected engineering fidelity and computational times. This analysis showed that the IDS simulated the transient development of the expanded jet flow, while revealing the formation, growth and instability of Kelvin-Helmholtz structures within the mixing layer. Further, the 2D IDS results were compared to results simulated by high fidelity techniques, such as, 2D URANS and LES studies, leading to the conclusion that the IDS 2D results closely matches LES analyses. In this paper, both inviscid and viscous analyses were successfully conducted, but at the time of publication, the perturbations studies were still ongoing.

I. Nomenclature

d_S = Surface Element
d_V = Volume Element
E = Internal Energy Pre-Unit Volume
F_{inf} = Inviscid Force
F_{vis} = Viscous Force
P = Pressure
ρ = Density
τ = Shear Stress
t = Time
T = Temperature
u = x-Velocity Component
U = Time Flux Vector
v = y-Velocity Component
w = z-Velocity Component

II. Introduction

The physics of under-expanded supersonic jet fluid field have drawn considerable interest in the aerodynamic design community. Most recently, this highly unsteady compressible flow field has been studied in numerous computational fluid dynamic (CFD) schemes. Many of which involved the use of unsteady Reynolds Average Navier-Stokes (URANS) equations, Large Eddy Simulation (LES) techniques, Direct Numerical Simulations (DNS) techniques and even the recently developed Gas-Kinetic Scheme (GKS) [1-2]. In general, the most capable of these CFD simulations showed the under-expanded flow field features consist of the main vortex pair, the vortex-induced shock waves, expansion waves, shock-vortex interactions, and Kelvin-Helmholtz type structures and their evolutions. However, what is still uncertain at this point, is the CFD requirements needed to effectively evaluate this highly transient flow field with the goal of understanding the effects of an initial perturbation on the interaction of vortex-induced shock with the jet shear layer in efforts to accelerate the instability and mixing of the shear layer.

In other words, now that the unsteady under-expanded jet flow features are revealed [3-8], is it possible to efficiently simulate the manipulation the Kelvin-Helmholtz structures within the mixing layer to study the instability characteristics of the resulting mixing layer. The 2D inviscid and viscous studies conducted herein revealed the unsteady flow structures associated with the under-expanded jet flow. Further, the Integro-differential scheme [9-10] (IDS) simulations captured most of the significant flow features along with their unsteady interactions within the core vortex. The IDS [11] solution was compared to the LES computations in Ref. 1, and the results were found to be are very similar.

III. Les Evaluation of Under-Expanded Jet

Consider the LES study the under-expanded flow field conducted in Ref. 1, and its main result which is illustrated in Figure 1 [1]. As observed, the primary shock wave (not shown in Figure 1) first exits the nozzle and it is immediately followed by a slightly expanding flow around the edges of the nozzle. The resulting behavior of these two actions, initiates the creation of a well-defined shear layer. The shear layer grows as it traps the rapidly exhausting core supersonic flow as it barrels out the jet. As this flow field develops, the resulting shock wave, expansion wave, shear layer interactions lead to the misalignment of the pressure and density gradients fields, which in turn creates a shear layer rolls to an ever-growing vortex ring. Once fully formed, the vortex ring moves downstream in the form of a mushroom head [1].

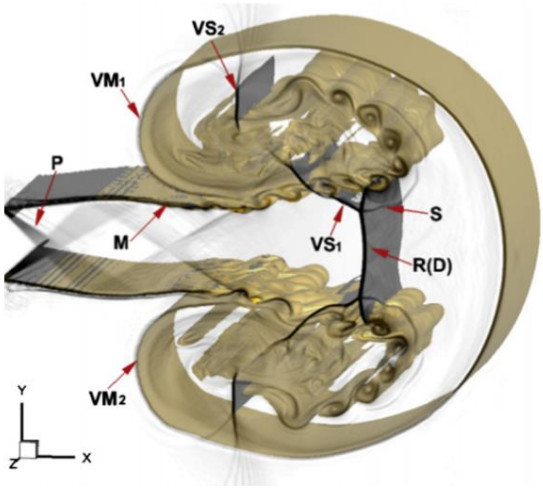

FIGURE 1: SCHLIEREN IMAGE OF FLOW STRUCTURE WITHIN A 2D UNDER-EXPANDED JET FLOW [1].

Again, refer to Figure 1 [1], but now knowing that it highlights the main result of the LES study in the form of the flow field features of interest to the aerodynamicist. A close observation of the field indicates the presence of Prandtl–Meyer expansion waves at the immediate exit of the jet, which is depicted by the letter P in the diagram. The shear layers are highlighted with the letter M, and their formation and evolution are clearly visible. In addition, the formation, evolution and transition of the Kevin-Helmholtz instabilities within these shear layers dominate, until they interact and transform into the two main or core vortices, labelled VM. Again, refer to Figure 1. Also captured within the core jet flow are the reflecting expansion waves and the terminating normal or diaphragm shock wave, which is indicated by the letters R(D). The diaphragm or normal shock wave terminates by interacting with the shear layer

which at this time is dominated by the Kevin-Helmholtz flow structures. The termination process of the diaphragm shock wave R(D) splits the ends of this normal shock into two weaker pieces, each labelled by the letters VS_1 and VS_2 with each terminating within their respective core vortex.

As the flow field further develops, the vortex ring expands by entraining larger regions of the surrounding ambient gas, resulting into a core vortex pair [12-18] with a fast-growing diameter. Previous studies showed that this vortex ring plays an important role in the formation of the shock-cell structures within the vortex core. Unfortunately, in the case of a supersonic under-expanded jet, the complicated shock patterns and their unsteady development is still not fully understood, especially when it comes to manipulating its behavior to enhance mixing. This CFD study seeks to investigate the physics within the developing under-expanded jet flow with the goal of understanding the vortex ring structures and the interacting flow features within them. Further, the numerical tool of choice is the Integro-Differential Scheme, which has shown that it is capable of capturing detailed flow field physics over long intervals of time [9-11].

IV. The Integro-Differential Approach

An improved finite volume approached, called the IDS, was formulated and implemented to primarily solve the integral form of the Navier-Stokes equations. The IDS was created from a physics-based perspective with a set of rigid assumptions, which allowed for all the integration terms in the conservation laws to be solved by the mean value theorem. The purposes of this section of the paper are (a) to provide a brief overview of the IDS with emphasis on its capability to solve compressible flow problems, and (b) to demonstrate the effectiveness of the IDS as a CFD tool to accurately solve complex engineering flow fields under realistic Mach and Reynolds number conditions. For further details on the IDS approach, consult Ref. [9-11].

A. The Integro-Differential Approach

The system of equations (1 - 3) collectively represent the mass, momentum and energy conversation laws that dictate fluid flows. For gas dynamics in particular, the equations (1 – 3) are coupled to the well-known viscous and Fourier relations, as well as, the equation of state to form a closed system of five equations relative to five unknowns. In this study the closed system of equations is referred to as the system of Navier-Stokes equations (NSE).

$$\frac{\partial}{\partial t}\iiint_V \rho dv + \oiint_S \rho \bar{V} d\bar{s} = 0 \tag{1}$$

$$\frac{\partial}{\partial t}\iiint_V \rho \bar{V} dv + \oiint_S \rho (\bar{V} \bullet d\bar{s}) \bar{V} = -\oiint_S P d\bar{s} + \oiint_S \bar{\pi} d\bar{s} \tag{2}$$

$$\frac{\partial}{\partial t}\iiint_V \rho E dv + \oiint_S \rho E \bar{V} \bullet d\bar{s} = -\oiint_S P \bar{V} \bullet d\bar{s} + \oiint_S \tau \bullet \bar{V} d\bar{s} + \oiint_S q \bar{} d\bar{s} \tag{3}$$

The symbols described in equations (1 – 3) are described in the nomenclature section. It is noteworthy to mention that the NSE provides a unique solution to a given fluid flow problem when the appropriate initial and boundary conditions are specified.

In the IDS formulation the NSE (1 – 3) is best described in the vector form,

$$\frac{\partial}{\partial t}\iiint_\vartheta \mathbf{U} d\vartheta + \oiint_S \overrightarrow{F_{inv}} \bullet dS + \oiint_S \overrightarrow{F_{vis}} \bullet dS = 0 \tag{4}$$

B. The Integro-Differential Approach

Consider the NSE in relationship to an elementary control volume. In accordance with the IDS formulation, the average flux, volume and surface quantities associated with the prescribed elementary volume are defined as,

$$\mathbf{U}_{\vartheta,avg} = \iiint_\vartheta \mathbf{U} d\vartheta \Big/ \iiint_\vartheta d\vartheta \tag{5}$$

$$\vec{F}^{n\pm}_{\text{inv , avg}} = \oiint_S \vec{F}^{n\pm}_{\text{inv}} dS \Big/ \oiint_S dS \tag{6}$$

$$\vec{F}^{n\pm}_{vis\,,\,\mathrm{avg}} = \oiint_S \vec{F}^{n\pm}_{vis}\, dS \,/ \oiint_S dS \tag{7}$$

where the symbol *U* represents the volumetric time flux vector. It is noteworthy to mention that all quantities of interest are either defined at the center of the control volume or on its surface. When the vector equation (4) is integrated over time for a fixed elementary control volume, an expression for the updated time-flux vector is obtained in the form,

$$U^{t+\Delta t}_{\vartheta,\,Avg} = \; U^{t}_{\vartheta,\,Avg} + \Delta t \left(\frac{\partial U}{\partial t}\right)^{t}_{\vartheta,\,Avg} \tag{8}$$

where the average time derivative in equation (8) is computed with the aid of expressions (9), such that,

$$\left(\frac{\partial U}{\partial t}\right)^{t}_{\vartheta,Avg} = \left\{ \left(\oiint_s \left(\vec{F}_{inv}\cdot\vec{n}\right) ds + \oiint_s \left(\vec{F}_{vis}\cdot\vec{n}\right) ds \right) / \oiiint_v dv \right\} \tag{9}$$

The computational concept summarized above is called the Integro-differential scheme (IDS). It's detailed formulation and error analysis, along with the results of its application to selected Quasi-1D, 1D and 2D problems are presented in Ref. 9 - 11.

C. Explicit Time Marching Process

For illustrative purposes, the 3D explicit time marching process associated with the IDS scheme is conducted on an 'equivalent Taylor series expansion' formulation as follows:

$$U^{t+\Delta t}_{i,\,j,k} \;\; = \;\; U^{avg,t}_{i,\,j,k} + \left(\frac{dU}{dt}\right)^{avg,t}_{i,\,j,k} \Delta t \tag{10}$$

where the time flux vector, U, is defined at each *ijk*-point, such that, $U = \begin{bmatrix} \rho & \rho u & \rho v & \rho v & \rho E \end{bmatrix}^T$. The terms on the right of equation (10) are not defined at an *ijk*-point but rather from the control volume and the temporal cell associated with each ijk-point. The term, $U^{avg,t}_{i,j,k}$, is the average value of the flux quantities associated with the control volume surrounding the *ijk*-point. Whereas, the time derivative term in equation (10) is associated with the average rate of change of temporal fluxes associated with the temporal cell at the *ijk*-point. For time marching purposes, the unsteady solution is advanced at each time step using the RK3 TVD algorithm as follows [19]:

$$\begin{aligned} \mathrm{u}^{(1)} &= \mathrm{u}^{\mathrm{n}} + \Delta t\, \mathrm{L}\left(\mathrm{u}^{\mathrm{n}}\right) \\ \mathrm{u}^{(2)} &= \frac{3}{4}\mathrm{u}^{\mathrm{n}} + \frac{1}{4}\mathrm{u}^{(1)} + \frac{1}{4}\Delta t\, \mathrm{L}\left(\mathrm{u}^{(1)}\right) \\ \mathrm{u}^{\mathrm{n+1}} &= \frac{1}{3}\mathrm{u}^{\mathrm{n}} + \frac{2}{3}\mathrm{u}^{(2)} + \frac{2}{3}\Delta t\, \mathrm{L}\left(\mathrm{u}^{(2)}\right) \end{aligned} \tag{11}$$

Finally, it is of interest to note that unlike most CFD numerial integration process, in this scheme, the time increment is not necessarly a function of the grid spacing, ie. $\Delta t \neq f(\Delta x)$. In the case of the IDS formulation, the time interval for each advcement is computed is a manner consistent with the elementry processes within an elementary control volume. The IDS scheme described herein can be implemented in either the inviscid or the viscous formulation.

V. An IDS Analysis of the Supersonic Jet

The problem of interest to this paper was already solved in Ref. [1] using the high fidelity CFD LES simulation technique, and its main results illustrated in Figure 1. Further, Figure 1, clearly highlights the expected nature of the under-expanded jet flow along with the many complex transient interactions that eventually leads to the buildup of the flow features illustrated in Figure 1. The basic problem of interest to the IDS analysis at this stage is simply this:

Can the numerical formulation which was described in the previous section generate the flow field features illustrated in Figure 1, under the same set of prescribed conditions?

A. IDS Problem Definition

In general, the mixing layer, the shear layer, the expansion fans, the shock wave interactions, and the formation of the main vortex within the under-expanded jet flow are all highly dependent on the nozzle shape, the exit Mach numbers [20], the density ratio and the ambient conditions surrounding the nozzle exit. In this paper, a 2D model was created from the conditions provided in Ref. 1. All computational aerodynamic and domain data of interest to the IDS formulation was directly computed from the aerodynamic and geometric data provided in Ref. 2. The height of planar nozzle is h = 0.01 m, and its width, L_z = 4h. The length of the domain is 10h and the height is 10h. The Freestream Gas Dynamic Parameters of interest to the IDS simulation are tabulated in Table 1, and the Jet Entrance Flow Conditions are tabulated in Table 2.

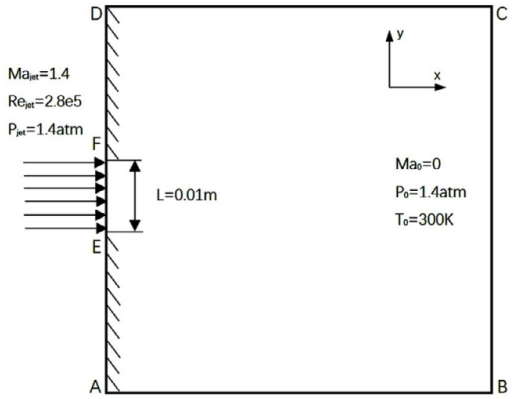

FIGURE 2: ILLUSTRATION OF THE IDS UNDER-EXPANDED JET COMPUTATIONAL DOMAIN.

Table 1. Freestream Gas Dynamic Parameters

Parameters	Ambient Conditions
Freestream Temperature	300.00 K
Total Pressure	1.4 atm
Temperature Velocity	0.0 m/s
Speed of Sound	340.174 m/s
Viscosity	$1.73 \times 10^{-5}\ m^2/s$

Table 2: Entrance Jet Flow Parameters

Parameters	Values
Mach at Entrance	1.4
Temperature at Entrance	300 K
Pressure at Entrance	1.4 atm
Ratio of Specific Heats	1.4
Reynolds Number	2.8×10^5

B. Boundary Conditions & Grid Densities

In accordance with the under-expanded LES model described in Ref. 1, the following boundary conditions [21] were applied to the IDS 2D under-expanded jet model:

1) Non-reflective boundary conditions were applied to the far-field and outflow boundaries (including the top, bottom and outlet planes),
2) Solid viscous wall boundary conditions were applied to the upper and lower walls of the planes directly above and below the nozzle, as appropriate for inviscid and viscous studies,
3) Constant velocity components, temperature and density conditions were applied at the nozzle exit zone, and
4) The flow field simulations were carried out under three sets of grids; 1001 by 1001, 2001 by 2001and 6001 by 6001 for inviscid and viscous cases, respectively.

C. Grid Independence Studies

Three sets of uniform Cartesian grids were used for meshing the computational domain and evaluating the physics within the jet flow. The following grid sizes were used to test the independence of the IDS grids [22]: a course grid size of 1001 by 1001, a medium grid size of 2001 by 2001 and a fine grid size of 6001 by 6001. In the IDS physical domain, these grids are labelled as Coarse, Medium and Fine grids, respectively. In addition, for each grid set the unsteady solution was allowed to run for 12 non-dimensional units. After each run, the computed solutions were analyzed with the goal of studying the influence of the grid sizes on the solution accuracy. The non-dimensional density and u-velocity distributions along the y-mid centerline of the inviscid under-expanded flow field are illustrated in the over-plots illustrated in Figures 3a and 3b, respectively. These plots indicate that the simulated inviscid flow fields are independent of their grid densities.

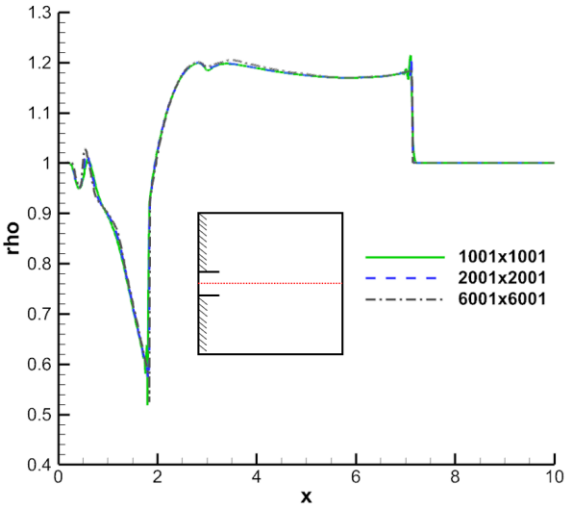

FIG 3A: INVISCID DENSITY PLOTS FOR GRID INDEPENDENCE STUDIES

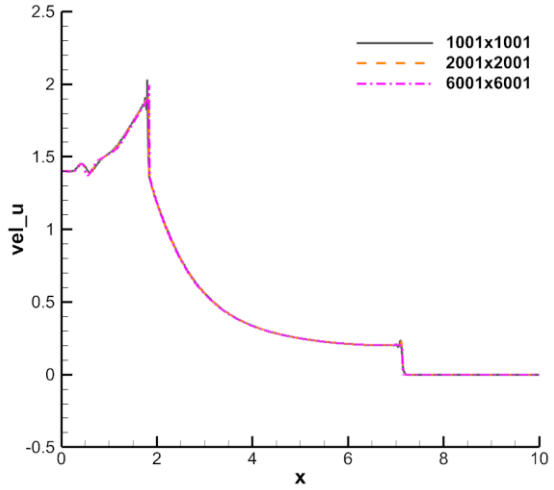

FIG 3B: INVISCID U-VELOCITY PLOTS FOR GRID INDEPENDENCE STUDIES

In a similar manner, viscous grid independence studies were conducted on the course, medium and fine grids in the forms of non-dimensional density and u-velocity distributions plots for a non-dimensional time of 12 at the y-mid centerline. These plots are comparatively illustrated in Figures 4a and 4b. Again, it can be seen that the fine and coarse plots produce similar results. Finally, the vorticity contour maps, for the inviscid and viscous cases, at the non-dimensional times of 9, 11 and 12 units were analyzed and compared to the LES simulations conducted in Ref. 1. The results of this analysis are tabulated in Table 3. A close look at the data illustrated in Table 3 indicated that the fine grid, 6001 by 6001, is the best choice for the study proposed herein.

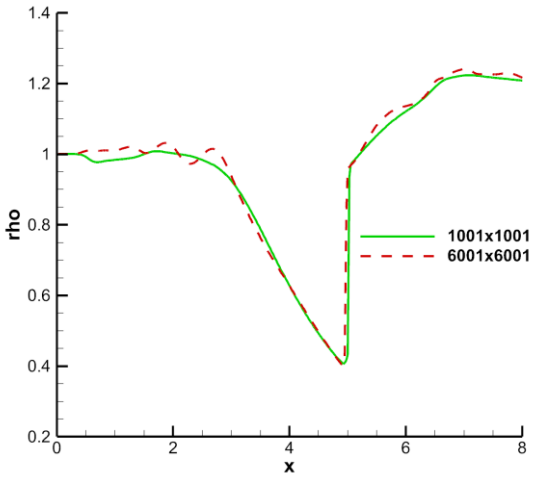

FIGURE 4a: VISCOUS DENSITY PLOTS FOR GRID INDEPENDENCE STUDIES

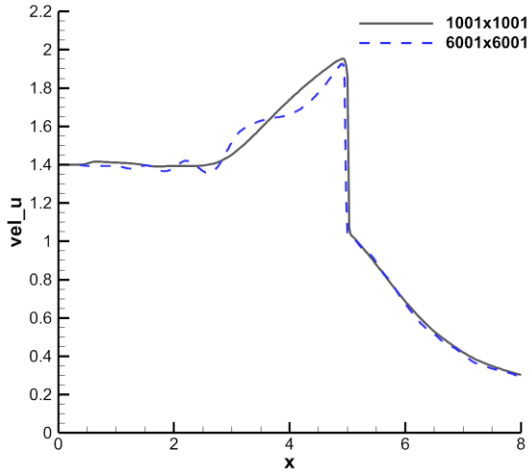

FIGURE 4b: VISCOUS U-VELOCITY PLOTS FOR GRID INDEPENDENCE STUDIES

Table 3: A Comparative View of the IDS and LES Vorticity Maps in the Under-expanded Jet

Time	Vorticity IDS	Vorticity LES
$\bar{t}$ = 9.0	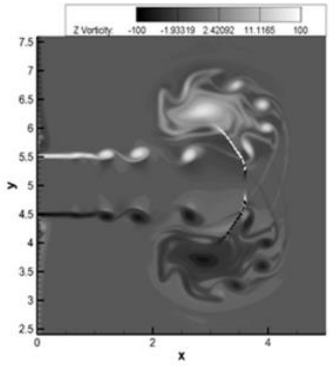	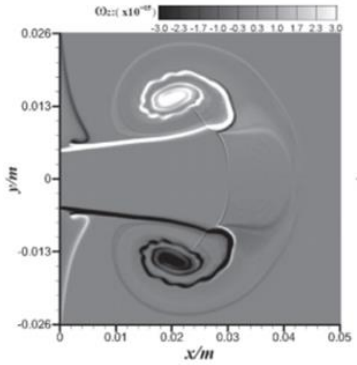
$\bar{t}$ = 11	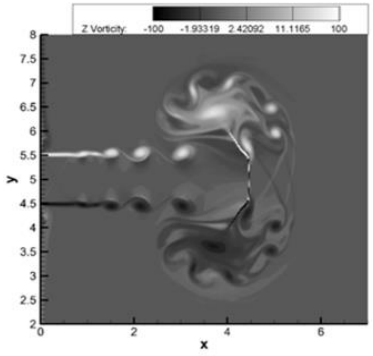	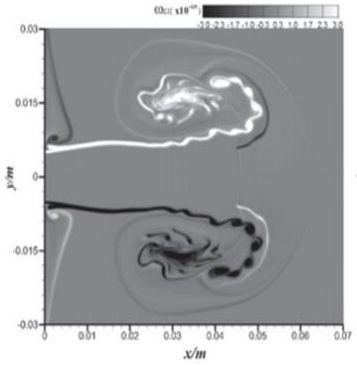
$\bar{t}$ = 12	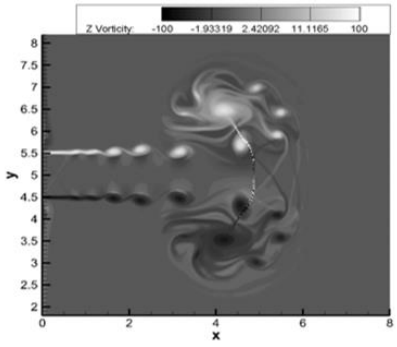	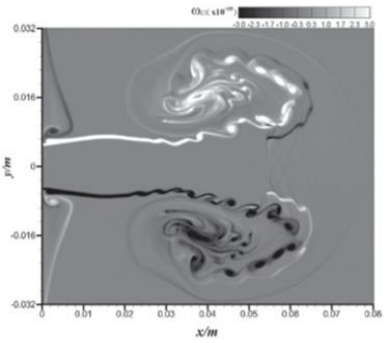

VI. IDS Simulated Results and Discussions

The unsteady under-expanded flow fields, in the form of density gradient distributions on the fine grid, at the non-dimensional time of 12 units obtained from the GKS, IDS Inviscid and IDS Viscous simulations, are illustrated in Figures 5a, 5b and 5c, respectively. Qualitatively, both of the IDS CFD simulation results in the form of density gradient distribution, compared very well with the GKS solution developed in Ref. x. In each of the two IDS cases, the under-expanded flow field features consist of the main vortex pair, the vortex-induced shock waves, shock-vortex interactions, and Kelvin-Helmholtz type structures and their evolutions. It is noteworthy to mention that the IDS flow field structure, in the case of the IDS Inviscid simulation, appears to be better resolved when compared to the IDS Viscous case. In a similar manner, the acoustic signature of the flow field, the inviscid case is again very well resolved when compared to the viscous case. However, these questions can be answered with further grid refinement analysis.

It is now time to qualitatively evaluate the IDS solution in relations to the available LES data. The following two sections, **Section VI.A** and **Section VI.B**. **Section VI.A** seeks to qualitatively illustrate the unsteady flow features captured by the IDS for the Inviscid and Viscous cases, and **Section VI.B** seeks to quantitatively compare the IDS results with the LES data in efforts to access the veracity of the IDS scheme.

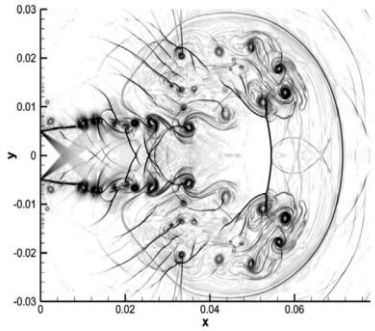

Fig. 5a: GKS Simulation, Ref. 2

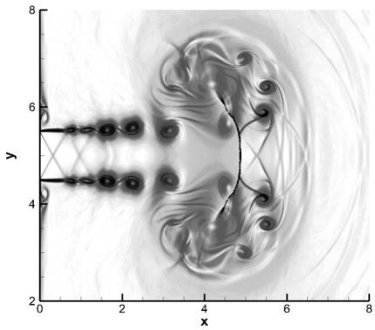

Fig. 5b: IDS Inviscid Simulation

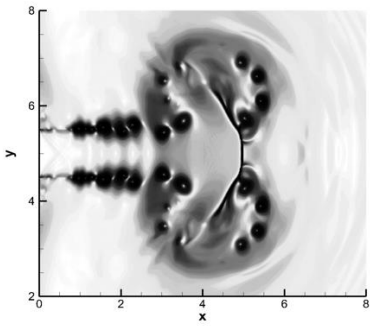

Fig. 5c: IDS Viscous Simulation

A. Analyzing the IDS Unsteady Results

The IDS Inviscid and Viscous solutions of the unsteady under-expanded jet flow problem, for non-dimensional time varying from 0 to 12, were analyzed on the fine grid, and the two cases compared at selected fixed times. For illustrative purposes in this paper, only the data for non-dimensional times of 5, 7 and 11 are tabulated and compared. Nevertheless, the conclusion drawn from this analysis is applicable for all times from zero to 12 non-dimensional units.

The results of interest to this section are tabulated in Table 4. A close observation of the data in Table 4 for a non-dimensional time of 5 units, reveals that the initial shock wave traveled further and faster in the inviscid case when compared to the viscous case. For times greater than 6 units, the primary shock had already departed the flow field. In addition, for all times, the shadowgraphs indicated that the inviscid data appears to be nosier when compared to the viscous cases. It can be clearly observed that the acoustic waves in the inviscid cases dominates the flow field. Again, in all cases, it seems that the fine grids, resolved the inviscid flow physics in a much clearer manner when compared to its viscous counterpart. Nevertheless, it is of interest to note that in every instance, the viscous flow cases captured the minute details associated with the Kelvin-Helmholtz fluid structures.

It can be clearly observed in Table 4 that in the viscous cases more coherent flow structures were captured, as well as, their interactions better preserved when compared to the inviscid cases. This conclusion is supported by the GKS results illustrated in Figure 5a, where the viscous case delivered the same amount of coherent flow structures that the GKS method predicted. Also, in the viscous cases, the primary and secondary shockwaves are better resolved when compared to the inviscid cases. In addition, the secondary normal shock wave interactions with the vortex pair yield the expected lambda-behavior, which is absent in the inviscid cases.

After observing the unsteady flow field simulations generated by the IDS computational technique, it can be concluded that the primary shock wave initial leaves the jet exit and races ahead of the flow field. This is true for both cases, inviscid and viscous. Next, the Prandtl-Meyer expansion waves followed, and then the shear/mixing layer phenomena begins. As can be observed in each shadowgraph, the vortex begins to gentle roll up as the core exhaust gas shoots itself into the ambient flow field. As time progresses, the width between the two shear layers seems to remain constant, confining the core flow to a ‘constant area’ duct, in which the Prandtl-Meyer expansion waves reflect between its two surfaces and culminating in a terminal normal shock. In addition, as the length of this ‘constant area’ duct grows, it can be observed that the Kelvin-Helmoltz vortices appear and rapidly evolves as well. It is of interest to note, the Kelvin-Helmoltz vortices are highly unstable, but nevertheless, the IDS numerical method is accurate enough to capture the details associate with these structures.

Again, it can be observed that the accuracy of the simulated results is also maintained as these Kelvin-Helmoltz vortices are processed by the terminating normal shock wave in the core flow.

Table 4: A Comparative Evaluation of the IDS Unsteady Jet Shadowgraphs

Time	INVISCID SHADOWGRAPH	VISCOUS SHADOWGRAPH
$\bar{t} = 5$	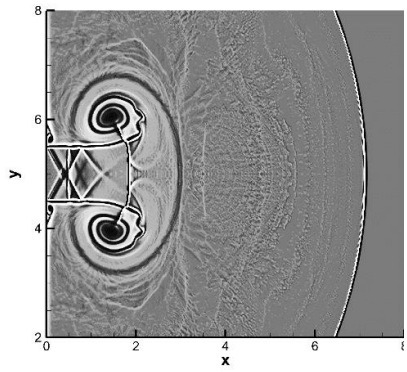	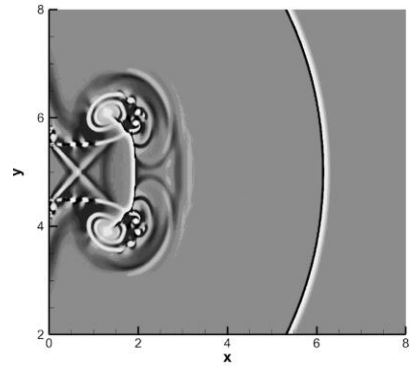
$\bar{t} = 7$	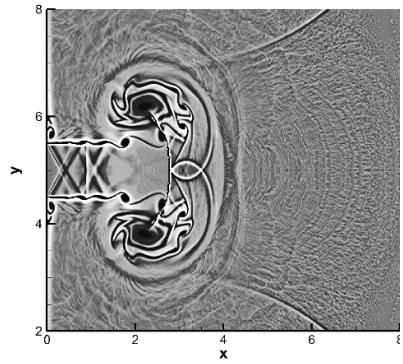	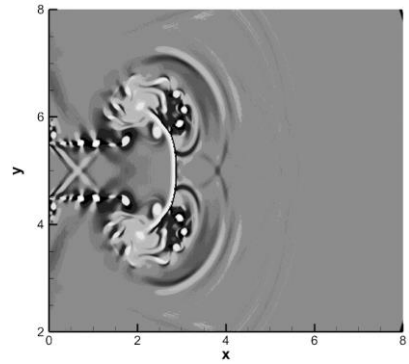
$\bar{t} = 11$	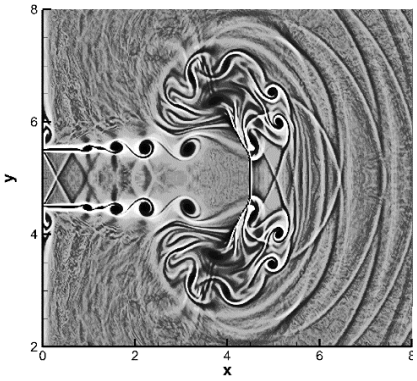	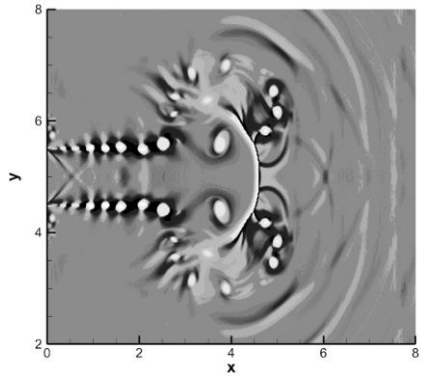

B. Analyzing the Unsteady Inviscid and Viscous Flow Physics

Consider the IDS inviscid and viscous simulations results illustrated in Figures 6a and 6b. These results, in the form of density gradient maps, represent the under-expanded flow field at a non-dimensional time of 12 units. These simulations provide a complete picture of the inviscid and viscous flows; illustrating the expansion fans (P) and their reflections as the jet enters the outer flow field, along with the creation of the confined jet flow held between the two developing shear layers (M) that eventually terminates into a pair of vortices (VS) and a normal shock (R). In each case, it can be observed that Kelvin-Helmoltz type-structures were created and rapidly grew within the shear layers, and even allowed to penetrate the terminating normal shock wave before coalescing into the main vortex. In both Figures 6a and 6b, it can be observed that the Kelvin-Helmoltz vortices, even though distorted as they pass the terminating normal shock, they hold onto their Kelvin-Helmoltz type-structures but now begin to rap themselves into forming the main core vortex, which will become the main vortex and lend themselves to a common core. It can also

be observed that the shadowgraph of the IDS viscous flow field is not well resolved when compared to its IDS inviscid counterpart. This question will be answered when fines grid are employed and other flow field characteristics filter are employed.

Nonetheless, the similarities of the two IDS simulated flow field structures to the one described in Figure 1 is remarkable. It is clear that the shadowgraph plots illustrated in Figures 6a and 6b, deliver the completed formulation of the core vortex pairs with all the expected flow field features that are expected in a typical under-expanded jet flow. The main vortex pair, described earlier by VM_1 and VM_2 in Figure 1 can now be clearly observed. In addition, the Prandtl-Meyer expansion waves, described by the letter P, as well as the shear/mixing layers, described by the letter M in Figure 1 can also be recognized. In addition, the terminating shock in the core flow described by the letter R in Figure 1 is also captured. Also, vortex-induced shocks pair (VS1 and VS2) locates on opposite sides of the shear layer of the vortex core are also captured.

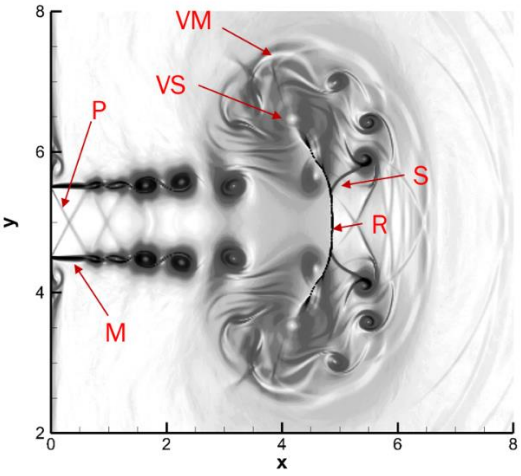

FIGURE 6a: IDS inviscid flow field schlieren

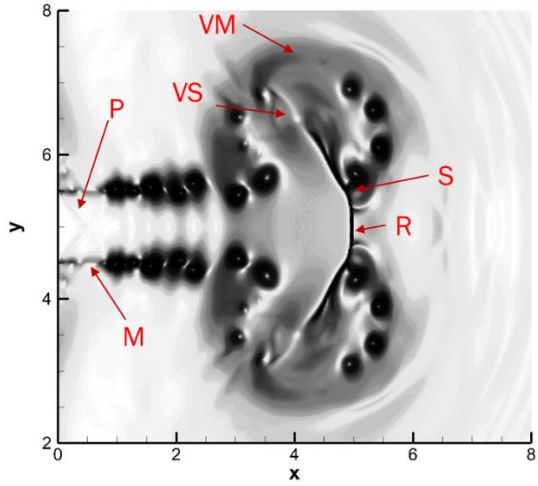

FIGURE 6b: IDS viscous flow field schlieren

C. IDS and LES Comparative Results

Now, consider Figures 7a and 7b. The local 1D plots of the u-velocity and pressure profiles along the x-center of the core vortex as contained from the LES [1] and IDS viscous simulations, are illustrated in Figures 7a and 7b, respectively. It is of interest to note that the LES solution in Figure 7a is expressed in dimensional quantities, while the IDS viscous simulated results are expressed in non-dimensional quantities. Nevertheless, the behavioral characteristics of these plots are very similar. In the case of the pressure plots, the vortex behavior [23-24] may be considered identical.

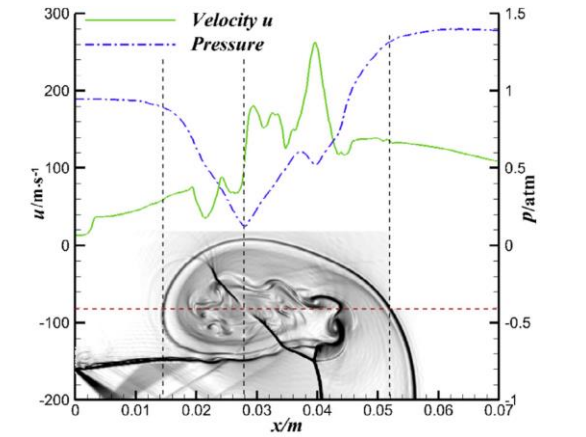

FIGURE 7a: LES VELOCITY AND PRESSURE PROFILES

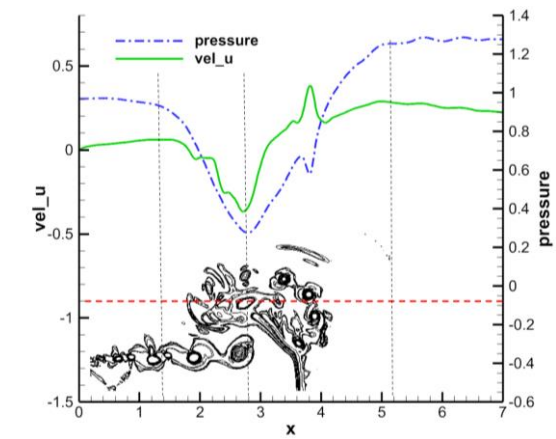

FIGURE 7b: IDS VELOCITY AND PRESSURE PROFILES

If one were to consider the fact that the flow features, such as, density, density gradient, entropy, and vorticity, were akin to filters, then it can be clearly shown that each filter reveals the physical details within the flow field in its rightfully independent but characteristic manner. However, they all tell the same common story, the IDS simulated results are consistent with the physical expectations of the flow field. More importantly, like the LES results, the IDS results captured the flow physics.

VII. Conclusion

The transient development of the under-expanded flow field produced by a supersonic jet was simulated through the use of a relatively new CFD technique called IDS. The geometric and aerodynamic data needed for the simulation of this problem was take from an LES study conducted in Ref. 1. Further, the IDS simulations were conducted on three sets of grids: a coarse, medium and fine grid, respectively. In addition, both inviscid and viscous simulations were conducted over a span of 12 non-dimensional unit. In addition, grid generation studies were conducted, and the results suggested that the fine grids (6001 by 6001 grid points) will be used for all subsequent analyses.

In this paper, both inviscid and viscous analyses were successfully conducted. The IDS solutions were mainly compared to simulations conducted in Ref. 1 and x. In general, the referenced CFD solutions showed the under-expanded flow field features consist of the following: the main vortex pair, vortex-induced shock waves, shock-vortex interactions, and Kelvin-Helmholtz type structures and their evolutions. In both cases; that of the inviscid and viscous, not only did the IDS simulations closely matches the GKS and LES results, they reflected the expected flow physics within the under-expanded jet. Moreover, this analysis showed that the IDS simulated the transient development of the expanded jet flow, while clearly revealing the formation, growth and instability of Kelvin-Helmholtz structures within the mixing layer. Further, when the 2D IDS results were compared to the results simulated by the high-fidelity techniques, it led to the conclusion that the IDS 2D results closely matches LES analyses. In this paper, both inviscid and viscous analyses were successfully conducted, but at the time of publication, the perturbations studies were still ongoing.

VIII. References

[1] Huanhao Zhang, Zhihua Chen, Xiaohai Jiang, Zhengui Huang, The starting flow structures and evolution of a supersonic planar jet, Comput. Fluids 114 (2015) 98–109.

[2] Xing Ji, Fengxiang Zhao, Wei Shyy, Kun Xu, A family of high-order gas-kinetic schemes and its comparison with Riemann solver based high-order methods, Computational Physics 356 (2018) 150-173.

[3] Bulent K, Otugen MV. Scaling parameters for underexpanded supersonic jets. Phys Fluids 2002; 14:4206–15.

[4] S Tsutsumi, S Teramoto, K Yamaguchi, T Nagashima, Structure of underexpanded jets from square nozzles, AIAA journal, 2006.

[5] TJS Jothi, K Srinivasan, Role of initial conditions on noise from underexpanded pipe jets, Physics of Fluids, 2009.

[6] V. Vuorinen, J. Yu, S. Tirunagari, O. Kaario, M. Larmi, C. Duwig, and B. J. Boersma, Large-eddy simulation of highly underexpanded transient gas jets, Physics of Fluids 25, 016101 (2013).

[7] H Zhang, Z Chen, X Jiang, H Li, Investigations on the exterior flow field and the efficiency of the muzzle brake, Mechanical Science and Technology volume 27, pages 95–101 (2013).

[8] R Mariani, MK Quinn, K Kontis, A note on the generation of a compressible vortex rings using helium as driver gas, Proc IMechE Part G: J Aero Eng 2012;227:1637–45.

[9] F Ferguson, Y Gao, D Feng, MD Atkinson, JC Mendez, Investigating the Unsteady Fluid Physics within Complex Flows Fields, AIAA Scitech 2021 Forum, 0750.

[10] F Ferguson, D Feng, Y Gao, A Computational Investigation of Vortex Flows Across Shockwaves, AIAA Scitech 2020 Forum, 0811.

[11] Ferguson, F., and Elamin, G., 2006, " A numerical solution of the NS equations based on the mean value theorem with applications to aerothermodynamics," Advanced Computational Methods in Heat Transfer IX, p. 97.

[12] VV Golub, Development of shock wave and vortex structures in unsteady jets, Shock Waves, 1994.

[13] JH Arakeri, D Das, A Krothapalli, L Lourenco, Vortex ring formation at the open end of a shock tube: A particle image velocimetry study, Physics of fluids, 2004.

[14] JO Dabiri, M Gharib, Starting flow through nozzles with temporally variable exit diameter, Journal of Fluid Mechanics, 2005.
[15] H Zare-Behtash, K Kontis, N Gongora-Orozco, Experimental investigations of compressible vortex loops, Physics of Fluids, 2008.
[16] H Zare-Behtash, N Gongora-Orozco, K Kontis, Effect of primary jet geometry on ejector performance: A cold-flow investigation, journal of heat and fluid flow, 2011.
[17] K Kontis, R An, D Kounadis, H Zare-Behtash, Head-on collision of shock wave induced vortices with a cylinder and a sphere, journal of heat and fluid flow, 2008.
[18] Huan-hao Zhang, Zhi-hua Chen , Xiao-hui Sun, Xiao-hai Jiang &Bao-ming Li, Numerical investigations on the thrust augmentation mechanisms of ejectors driven by pulse detonation engines, Combustion Science and Technology Volume 183, 2011.
[19] S Gottlieb, CW Shu, Total variation diminishing Runge-Kutta schemes, Mathematics of computation, 1998.
[20] W Zhao, SH Frankel, LG Mongeau, Effects of trailing jet instability on vortex ring formation, Physics of Fluids, 2000.
[21] MB Giles, Nonreflecting boundary conditions for Euler equation calculations, AIAA journal, 1990.
[22] Frederick Ferguson, Dehua Feng, Yang Gao, Julio C Mendez, David DodooAmoo, Investigating the Computational Errors of Integral Schemes Through the Use of Numerical Experiments, AIAA Scitech 2019 Forum.
[23] H Zhang, Z Chen, B Li, X Jiang, The secondary vortex rings of a supersonic underexpanded circular jet with low pressure ratio, European Journal of Mechanics-B/Fluids, 2014.
[24] R Hillier, Computation of shock wave diffraction at a ninety degrees convex edge, Shock waves, 1991.